

3-D inversion of complex magnetotelluric data from an Archean-Proterozoic terrain in northeastern São Francisco Craton, Brazil

Mauricio S. Bologna^{a,*}, Gary D. Egbert^b, Antonio L. Padilha^c, Marcelo B. Pádua^c, Ícaro Vitorello^c

^a *Instituto de Astronomia, Geofísica e Ciências Atmosféricas, Universidade de São Paulo, São Paulo, SP 05508-090, Brazil.*

^b *College of Earth, Ocean and Atmospheric Sciences, Oregon State University, Corvallis, OR 97331, USA*

^c *Instituto Nacional de Pesquisas Espaciais, São José dos Campos, SP 12201-970, Brazil*

* Corresponding author. Tel.: +55 11 3091 2776; fax: +55 11 3091 5034.

E-mail address: mbologna@usp.br (M.S. Bologna).

2016

SUMMARY

We present a magnetotelluric (MT) study in the northeastern part of the São Francisco Craton that encompasses an Archean-Proterozoic terrain, the Serrinha Block, breached by a rift basin developed mostly in Early Cretaceous times during the opening of the South Atlantic Ocean. Even though the MT sites are regularly spaced, the profiles have different orientations from one another, making the data distribution over the area highly uneven and therefore non-ideal for 3-D modeling. However, the dataset is very complex, with dimensionality analysis indicating prevalence of 3-D geoelectric structure. Results from 3-D inversion are evaluated for robustness and potentiality for yielding tectonic information. At upper crustal depths the resulting 3-D model is coherent with surface geology, whereas at mid and lower crustal depths more cryptic structures are revealed, likely of Paleoproterozoic age. The most striking features in the model are several strong ($\sim 1 \Omega\text{m}$) crustal conductors beneath the central part of the Serrinha Block, which we attribute to a Paleoproterozoic oceanic plate subduction and arc-continent collision event involving the Rio Itapicuru Greenstone Belt and the basement of the Serrinha Block. The west-dipping geometry of these conductors provides a constraint on subduction polarity and gives support to tectonic evolutionary models proposing that the Rio Itapicuru Belt was formed in an island arc environment.

Keywords: Cratons, South America, Crustal structure, Electrical properties, Geomagnetic induction.

1 INTRODUCTION

A multidisciplinary project (Instituto Nacional de Ciência e Tecnologia de Estudos Tectônicos – INCT-ET) has been conducted in the northeastern part of Brazil to investigate the crust and upper mantle of the Borborema Province and adjoining São Francisco Craton. The goal of these studies is to understand better the actual articulation of the amalgamated crustal blocks that comprise this region, and to clarify the processes that brought them together (Vitorello et al. 2013). This work presents results from a magnetotelluric (MT) survey in the northeastern part of the São Francisco Craton as part of the INCT-ET activities. The study area encompasses an Archean nucleus, which represents the basement of Paleoproterozoic greenstone belts, ruptured by a rift basin developed mostly in Early Cretaceous times during the opening of the South Atlantic Ocean. Details of structure and tectonic history are still poorly known (e.g. Teixeira et al. 2000; Barbosa & Sabatè 2004).

The dataset consists of 68 broadband MT stations collected in a series of six linear profiles, laid out to transect major known geological structures. Even though the MT sites are regularly spaced around 12 km apart, the profiles have different orientations from one another, making the data distribution over the area highly uneven. Profile data of this sort has traditionally been interpreted using 2-D modeling and inversion (accounting for distortion). This approach is a priori questionable in this area, as surface exposures of geologic structure exhibit variable orientation - as indeed do the profiles we have laid out to sample these structures. Previous MT studies at contiguous areas of the Borborema Province (Padilha et al. 2016) and initial examination of our processed MT data suggest very complicated 3-D structure. It is observed that many sites have diagonal components with magnitudes comparable to the usually larger off-diagonal components, nearly a quarter of the sites have phase curves that go out of quadrant, and tipper orientations vary significantly in space. Distortion and strike

analysis of the impedance tensors further confirm that the data are strongly 3-D.

Even considering that the site layout is less than ideal for a 3-D inversion, the complications of this dataset make this choice the most reasonable approach. Here we use the ModEM 3-D MT inversion code (Egbert & Kelbert 2012) to integrate data from six crossing profiles into a 3-D image of resistivity variations in the study area. Whereas the wide lateral spacing between profiles imposes limits on resolution in some of the domain, the inversion results in sensible images which reveal evidence for deep crustal conductive features that are coherent with the surface geology. These conductors most likely represent conductive phases in suture zones associated with the Paleoproterozoic assembly of the craton.

2 GEOLOGICAL OUTLINE

The northeastern São Francisco Craton has been considered one of the best preserved segments of Paleoproterozoic to Paleoproterozoic crust in the South American Platform (Almeida et al. 2000). This region exposes medium to high-grade metamorphic rocks and remnants of low-grade greenstone belts. Based predominantly on geological, geochemical and geochronological data, different units have been recognized. These units consist basically of two Archean blocks, namely the Gavião and Serrinha blocks, separated by a highly deformed Paleoproterozoic unit known as Itabuna-Salvador-Curaçá Belt (ISCB).

The main tectonic units in the core of our study area are shown in Fig. 1. Following Barbosa & Sabatè (2004), the main aspects can be summarized as follows. The Gavião Block, in the western end of the survey area, is composed mainly of gneiss-amphibolite associations and amphibolite facies tonalite-granodiorite orthogneisses dated at ca. 2.8-2.9 Ga, as well as Archean greenstone belts. The ISCB is composed of granulite rock facies that include tonalite, charnockite with basic-ultrabasic

enclaves, and less abundant supracrustal rocks. The Serrinha Block is the predominant unit in the survey area, occupying an elliptical area of about 17,000 km² in the center of the survey area. It is composed of medium-grade gneiss-migmatitic rocks, with ages spanning 2.8 Ga to 3.1 Ga. The Serrinha Block also includes ubiquitous Paleoproterozoic greenstone belts, of which the Rio Itapicuru Greenstone Belt (RIGB) is the most important.

Granitoids of variable chemical composition and deformation degree are observed in the Serrinha Block. Following Costa et al. (2011), these include slightly deformed, pre- to syn-tectonic 2163-2127 Ma granites, with medium-K calc-alkaline plutons (e.g. 2.15 Ga Nordeste Batholith), and undeformed late to post-tectonic alkaline 2111-2070 Ma plutons, of which the most representative is the Itareru tonalite. In addition to these two groups of rocks, elongated gneissic-migmatitic domes are observed in the central-south part of the Serrinha Block. The domes have a dominant N-S structural trend that deflects to an E-W direction in the south. Ages are scattered in some samples (e.g. 2.08 Ga to 3.16 Ga for the Ambrósio Dome) apparently due to remobilization and metamorphism (Rios et al. 2009).

The northeastern and eastern parts of the Serrinha Block are covered by rocks of the Sergipano Belt and the Tucano Basin, respectively. In the study area, the Sergipano Belt is composed mainly of undeformed to weakly deformed siliciclastic and carbonate sediments that were deposited in a shallow marine environment during the Neoproterozoic. The Tucano Basin is an asymmetric half-graben filled mostly with Late Jurassic to Early Cretaceous non-marine successions including conglomerates, shales, mudstones and sandstones. Maximum rift sedimentation (> 10 km) is found along the eastern portion of the central and southern Tucano Basin, but basin depths reduce abruptly to the west, across the Vaza-Barris transfer fault in the northern part of the basin.

3 TECTONIC EVOLUTION

The present-day configuration and the structural framework of the Archean and Paleoproterozoic rocks in the northeastern São Francisco Craton result from the closure of the Serrinha Block against the Gavião Block during the Paleoproterozoic (Barbosa & Sabatè 2004). However, tectonic relations are poorly constrained and proposed evolutionary models are still controversial. Some authors (e.g. Gaal et al. 1987; Silva 1992; Matos & Conceição 1993) have suggested that the initial stage of regional evolution involved the development of a wide ocean basin west of the ISCB, with eastward-dipping subduction of the oceanic crust, and simultaneous formation of a back-arc basin in which the rocks of the RIGB were generated. In this scenario, the ISCB could be either a cratonic remnant or part of the magmatic arc related to the subducting plate. Figueiredo (1989) proposed an alternative tectonic model, with the ocean basin east of the ISCB. Then, subduction of oceanic crust toward the west would be responsible for the development of the RIGB as a back-arc basin with the ISCB as the magmatic arc (oceanic or continental). Although in almost all proposed models the volcanic-sedimentary sequence of the RIGB is interpreted to arise in a back-arc environment, the location of the coeval arc has not yet been determined.

In the Neoproterozoic, the study area experienced two main tectono-magmatic events. During the Pan-African/Brasiliano orogeny, the convergence and collision of the São Francisco Craton with the Borborema Province resulted in the formation of the Sergipano Belt (Brito Neves et al. 1977). Around 642 Ma, the Serrinha Block, mainly its central-western part, and surroundings was affected by kimberlite magmatism probably derived from strongly metasomatized lithospheric mantle (Donatti-Filho et al. 2013).

The most recent event affecting the survey region is the rifting associated with the formation of the Tucano Basin, which is part of a regional extensional system in northeast Brazil that was operative

during the Mesozoic breakup of South America and Africa (Karner et al. 1992). Proposed evolutionary models are still a matter of debate, but generally invoke control by low-angle major crustal detachments (Ussami et al. 1986) or flexural isostatic response associated with magmatic underplating and uplift (Magnavita et al. 1994).

4 METHODS

4.1 MT data

The MT method uses simultaneous measurements of natural time variations in the magnetic field components (H_x , H_y and H_z) of the Earth and the orthogonal horizontal components of the induced electric field (E_x and E_y) for determining the resistivity distribution within the Earth. In this study, the five electromagnetic components were acquired using commercial broadband MT systems equipped with induction-coil magnetometers and non-polarizable lead-lead electrodes. The data set consists of 68 stations evenly spaced about 12 km, acquired along six intersecting 2-D profile lines, as shown in Fig. 1.

The record duration at each station was typically one to two days. The measured time series were processed using the robust code of Egbert (1997), resulting in high-quality estimates of the MT impedance and transfer functions of the magnetic field (VTFs) in the period range of 0.001-410 s for the majority of stations. Longer periods (up to 2000 s) were achieved in some sites, especially those from the profile S2.

Fig. 2 shows the MT results for three representative sites, displayed as sounding curves (apparent resistivity and phase) computed for all four components of the impedance tensor. Site ser004a is within the ISCB. Apart from some scattering at specific periods, associated with 60-Hz transmission lines and in the dead-band of the natural signal around 10 s, curves are smooth, and the data appear to be of good

quality. However, phase values for the xy -component go out of quadrant, exceeding 90° for periods higher than 1 s. In addition, the diagonal components are very well resolved, and are of the same order of magnitude as those of the off-diagonal components. From previous studies, these characteristics suggest that the data may be affected by complex 3-D geometry (e.g. Aizawa et al. 2014; Kuhn et al. 2014) or by electrical anisotropy (e.g. Heise & Pous 2003; Weckmann et al. 2003). Site ser010a, located in the Serrinha Block, has smooth responses along the entire period range for all components. The yx -component phases leave the first quadrant at a period of ~ 10 s as for the site from the ISCB, the responses at ser010a display large amplitude diagonal components. For site ser017a, located over the sedimentary basin, the curves are almost 1-D for periods shorter than 10 s, i.e. curves for xy - and yx -components have similar shapes and the diagonal responses are weak, with large relative error bars, at least compared with the previous two sites.

Fig. 3 displays observed pseudo-sections of apparent resistivities and phases for the profile S1 that were used in the 3-D inversion discussed below. The Tucano Basin is well characterized at high frequencies by low resistivities from sites between positions 140 km and 240 km. The most remarkable feature of the basin is probably a zone of low apparent resistivity at the yx -component in longer periods, perhaps reflecting a rapid deepening of the basin. In the other part of profile S1 MT responses are very complex. Abrupt changes of resistivity and phase are observed at neighboring sites. Furthermore, most of the stations display phases outside the normal quadrant in both components even at relatively short periods (~ 0.1 s). All of this provides evidence for 3-D complications (see supplementary material for amplitude and phase pseudo-sections for other profiles).

The VTFs are often represented graphically as induction vectors, which can be used to assess qualitatively the conductivity structure of the subsurface. For simple structures the vectors are orthogonal to lateral resistivity gradients; amplitudes are zero directly over conductive bodies or in a 1-D Earth. Fig. 4 displays the real components of the induction arrows for four different periods in the

study area. We have defined these vectors to point toward zones of higher conductivity, following the Parkinson convention. At a period of 0.3 s (Fig. 4a), most stations in the Tucano Basin have a weak induction vector response, consistent with the presence of highly conductive rocks and a locally 1-D horizontal stratigraphy. In the central part of the region, we observe some reversals in the vector directions, which is suggestive of shallow conductive bodies. However, the overall pattern is complex, with no clear strike even on individual profiles. At longer periods (Figs 4b-4d), the amplitude of the vectors in the Tucano Basin increases considerably. In addition, directions become consistent, varying smoothly from one station to another and also with period. As the general direction of the vectors is approximately perpendicular to the Brazilian coastline, we initially suspected a strong ocean influence on these vectors. However, 3-D forward modeling using realistic ocean bathymetry suggests a negligible coast effect this far inland (~200 km). At the eastern end of the basin, a reversal in the direction of the vectors is observed, implying that at least part of the anomalous conductive structure must be confined within the lateral limits of the basin.

4.2 Data Dimensionality

To more quantitatively evaluate the dimensionality of our dataset we have used the Groom-Bailey (GB) tensor decomposition (Groom & Bailey 1989). This technique determines simultaneously the geoelectric strike and the near-surface distortion effects using a least-squares approach, assuming a galvanic distortion model that consists of a 3-D surficial frequency independent distortion overlying a 2-D regional conductivity structure. One way of checking the validity of the GB model is by examining both spatial and frequency dependence of the distortion parameters. Fig. 5 displays multifrequency GB decomposition at each site in different period bands. At short periods (0.1-10 s) (Figs 5a and 5b) strikes at most sites are in agreement with the structural trend of the Gavião Block, ISCB and Serrinha Block.

However, while the MT responses might be locally considered 2-D, some abrupt changes in strike direction indicate an overall 3-D behavior. The strongest change in direction is observed in several stations located in the central part of the study area, within the surface limits of the Serrinha Block. For sites over the Tucano Basin, strikes tend to be more scattered. This behavior would be consistent with a nearly 1-D geoelectric structure of the basin for high frequencies, as suggested also by the small anisotropy between xy and yx phases of most stations. For longer periods (Figs 5c and 5d), a clockwise rotation in the strikes directions is observed for many sites in the western region of the Serrinha Block, clear evidence for period dependence of the distortion parameters. In some stations in which the parameters of the decomposition are weakly dependent on period, and strike direction is well defined, phases remain above 90° even after the decomposition. In the northern segment of the Tucano Basin the determined strikes are consistently aligned nearly to the N-S (or E-W, due to the inherent 90° indeterminacy of the strike direction). However, the strikes in the central-southern segment and in the adjacent area over the southeastern Serrinha Block present a complex pattern. Therefore, formal strike analyses show that there is no preferential strike for the dataset, further confirming that the study area is strongly 3-D.

4.3 3-D Inversion

We performed a set of 3-D inversions using the Modular system for Electromagnetic inversion (ModEM; Egbert & Kelbert 2012; Kelbert et al. 2014). The preferred model presented here resulted from the joint inversion of full tensor impedance and VTFs for the 68 stations shown in Fig. 1. Measured data errors were discarded in favor of relative error bounds. We assigned error bounds of 5% of $|Z_{xy}Z_{yx}|^{1/2}$ for all impedance tensor components and a constant value of 0.03 for VTFs. We included 13 periods from 0.01 to 3200 s, removing noisy impedance and VTFs data. The nominal grid spacing in

the central part of the domain is approximately 3 km (102 x 112 cells). We used 53 vertical layers starting from 50 m and increasing logarithmically with a factor of 1.1 for the first six kilometers increasing to 1.2 for the deeper layers. The preferred model was obtained using a homogeneous 100 Ωm half space as prior and starting model, fitting the full dataset to a normalized root mean square (nRMS) misfit of 3.12. The observed and predicted pseudo-sections of apparent resistivities and phases for the profile S1 are shown in Fig. 3. To assess robustness of model features, inversions were also run with different control parameters and subsets of data, for example using 33.3 Ωm and 300 Ωm prior models, and inverting impedance tensor and VTFs separately and together. All inversions were run using a grid coordinate system with the x -axis aligned with geographic north. Illustrative alternative models are discussed in the supplemental material.

5 THE 3-D MODEL

Fig. 6 displays plan views of our preferred model. The uppermost parts of the model are broadly coherent with the surface geology, at least where we have data constraints. At depths of 50 m (Fig. 6a) for example, high resistivities ($>1000 \Omega\text{m}$) are associated with Precambrian rocks of the Gavião Block, ISCB and Serrinha Block, while low resistivities are found in the sediments of the Tucano Basin. However, the ModEM inversion penalizes deviations from an assumed prior, so at these shallow depths the model only changes near the data sites; especially in between the profiles, the inverse solution reverts to the assumed prior resistivity level. Furthermore, some localized small conductive features probably result from the inversion trying to correct galvanic distortions, and therefore have no geological meaning. At depths of 2-3 km (Fig. 6b), the model becomes smoother, and even lower resistivities ($<10 \Omega\text{m}$) are associated with lower units of the Tucano Basin. At the north end of profile T1, near the latitude of $\sim 10^\circ \text{S}$ (Figs 6b and 6c), the basement high associated with the Vaza Barris

transfer fault coincides with a transition to a highly resistive structure truncating the conductive sediments to the south.

Beneath the Tucano Basin, close to its deepest portion, we also observe another zone of high conductivity ($\sim 10 \Omega\text{m}$) (C1 in Fig. 6c). This zone is comprised of two prominent conductive anomalies extending to depths of about 20 km (see also Fig. 7). Actually, these conductors seem to be associated with a thickening of the basin rather than a conductive basement structure. In fact, the electric anomalies coincide spatially with the maximum basin depocenter mapped using gravity, seismic refraction data and surface geology, which has been inferred to be deeper than 12 km (Milani & Davison 1988).

The most important features in the 3-D model occur in the central part below 10 km (C2 to C5 in Fig. 6c). These features consist of a set of low resistivity ($\sim 1 \Omega\text{m}$) anomalies distributed along the central-western portion of the Serrinha Block. The most strongly expressed is C3, which has a remarkable spatial coincidence with the Nordestina Batholith (see location N on Fig. 1). Fig. 7 shows an E-W model cross section that crosses the center of C3. The conductive structure is imaged as dipping to the west, with its top and bottom located at depths of 5-6 km and 25-30 km, respectively. Similar structures are seen in alternative inversions, such as the VTF inversion (Figs S10b and S11).

5.1 Deep model assessment

To assess the depth resolution of our data we performed a set of additional inversions, some results of which are shown here, with additional details in the supplementary material. During these inversions the resistivity of the bottom of the model was kept fixed below a series of specified depths, allowing us to assess the impact of these imposed constraints on data fit and model structure. Specifically, we performed four 3-D inversion runs with resistivity frozen below 30 km, 60 km, 80 km and 120 km. In

one of the inversions the resistivity of the frozen layer was set to 20 Ωm (see Fig. S14), whereas in the remainder (see Fig. 8), the resistivity was set to 100 Ωm .

The inversions frozen below 80 km and 120 km produce similar results. The upper parts of the models do not change significantly and their final nRMS misfits are very close (3.07 and 3.13, respectively) to the unconstrained model. In the model frozen below 80 km, there is perhaps a slight decrease in the magnitudes of the anomalies. For the model frozen below 60 km, the amplitudes of the anomalies become slightly stronger compared with those in the unconstrained model. Also, the geoelectric features of the Serrinha Block and adjacent Precambrian areas to the west tend to be placed at shallower depths, whereas the low resistivity below the Tucano Basin appears to extend a little deeper. But, even these changes are modest, except in the middle part of the study area, where a resistive window in the crust allows deeper resolution. Not surprisingly, the most significant changes in the upper parts of the model are observed when the top of the frozen layer is brought up to 30 km. The relative greater impact of the constraint in this case can also be seen by the more significant increase of the nRMS misfit to 3.53.

We conclude from these tests that there is little resolution of structure below 30 km. The presence of strong zones of enhanced conductivity in the upper 10 km, mainly beneath the Serrinha Block and the Tucano Basin, shields deeper structure. As a consequence, the contrast between lithospheric mantle between the eastern and western blocks is not well resolved by the available broadband MT data, and the mantle anomalies apparent in Fig. 7 should be considered with caution.

6 DISCUSSION AND INTERPRETATION

Our results demonstrate that relatively simple 3-D isotropic models can explain out-of-quadrant phases. It is not necessary to generate any special combination of shallow and deeper electrically anisotropic

zones with different anisotropy strikes, as exemplified by the 2-D models considered by Pek & Verner (1997). Indeed, the fact that relatively simple 3-D models can exhibit out-of-quadrant phases is increasingly clear from both forward model studies (e.g. Ichihara & Mogi 2009), and from growing experience with 3-D inversion. Although the very complex impedances in this area are reproduced quite well (see Fig. 3 and Figs S1-S5), normalized misfits are somewhat larger (Fig. S8a) than in other areas, or in VTFs. Given this very challenging data set, we consider the overall misfit reasonable. Even problematic sites, with nRMS larger than six, are at least fit qualitatively (Fig. S8b). Nevertheless, amplitudes of both data and fitted are sometimes quite small that details (and phases) are not very meaningful, and differences are actually not great in an absolute sense.

In the study area, the main zone of out-of-quadrant phase is over the complex buried conductive features, and almost always just west of the exposed RIGB (Fig. 9). This appears most strongly in the yx mode, principally when x is aligned with N23°W, probably the local strike direction. This behavior of the phases is also evident over a range of rotations covering $\sim 45^\circ$, and at some sites out-of-quadrant phases occur in both polarizations. Consequently, we cannot eliminate these anomalous phases from inversions.

A second area of anomalous phase occurs along the western half of the profile S2. This is more sensitive to rotation, and vanishes for the N23°W case (i.e. the rotation for which the other area is strongest). Map views of phases for different coordinate rotations are shown in the supplemental material.

Given that melts and saline fluids would not be expected in a cratonic area, explanations for enhanced conductivity in stable deep crust usually invoke the presence of an interconnected network of iron sulfides and graphite (Jones 1992; Nover 2005; Selway 2014).

These explanations are likely relevant here as well, especially given the extensive literature on the role of subduction in the Paleoproterozoic geotectonic evolution of the study area. In fact, MT results

from ancient and modern subduction and/or collision zones in many parts of the world have shown that suture zones resulting from the accretion of terrains very often produce strong conductive anomalies in the lithosphere (see reviews by Jones 1993; Unsworth 2010; Selway 2014). The most salient of these features in ancient subduction zones are dipping layers of high conductivity observed along terrane boundaries. These are often interpreted as resulting from emplacement of metamorphic rocks at deep levels favoring the formation of a network of interconnected graphite or sulfide on a regional scale (e.g. Boerner et al. 1996; Wannamaker 2005).

The geometry of these conductive features can provide a primary constraint on the polarity of the subduction zone. Fig. 10 gives a more regional view of the resistivity distribution in the study area. It shows that similar west-dipping geoelectric features are observed beneath the central part of the Serrinha Block in several different vertical sections. We therefore suggest that this geometry provides a first-order constraint on a westward subduction polarity during Paleoproterozoic collision.

This interpretation is supported by several geologically-based lines of evidence for ancient subduction in this area. Geochemical analyses (Ruggiero & Oliveira 2010) of andesites and dacites from the RIGB have revealed adakites, typically produced by partial melting of hydrous metabasalts related to flat-slab subduction (Gutscher 2000). The position of these rocks to the west of a group of calc-alkaline affinity suggests westward subduction (Ruggiero & Oliveira 2010), consistent with the general inclination of the Serrinha conductors. Note that the production of adakitic magmas is almost always linked to flat subduction (Smithies et al. 2003), in agreement with the low-angle dip of the MT anomalies.

Subduction processes have also been invoked as a possible mechanism for formation of the Nordeste Batholith, whose trondhjemitic magmas are believed to result from partial melting of a Paleoproterozoic subducted ocean slab (Cruz Filho et al. 2003). Therefore, both adakitic and tonalite–trondhjemite–granodiorite magmas could have resulted from different stages of the same subduction

process. Moreover, mafic-ultramafic rocks have been observed approximately along the contact between the banded gneisses and the supracrustal rocks of the RIGB (Oliveira et al. 2007). These rocks are serpentinites with interstitial augite and minor chromite, presenting geochemical characteristics similar to ophiolitic complexes found in the Alpine-Apennine orogenic belts. Oliveira et al. (2007) have interpreted this complex as related to rifting of a magma-poor continental margin that preceded the closure of the Rio Itapicuru ocean basin. Because the age of this complex is poorly constrained, ranging from 2085 Ma to 2983 Ma, we suggest these rocks might alternatively represent oceanic crustal fragments trapped during the RIGB arc-collision event at about 2.1 Ga.

Additional support for a subduction explanation for the conductivity anomalies in the Serrinha Block is the fact that the late- to post-tectonic alkaline rocks in this region may have been generated as a consequence of slab breakoff, as suggested by Oliveira et al. (2010) and Rios et al. (2009) for the formation of the Itareru tonalite (see Fig. 1 for location). According to these authors, this event would have provided the thermal pulse required to melt a previously enriched mantle and generate the tonalitic magmas.

In the ISCB, the model also shows the presence of strong conductors (C6 and C7 in Fig. 6c). But unlike the features C2-C5, these anomalies are relatively localized and might be associated with mineralized zones in the belt.

Other important features of our model are two strong conductors in the southern part of the Serrinha Block (C8 and C9 in Fig. 6c). It is unclear whether these anomalies have a genetic relation with the anomalies C2 to C5 in the central part of this block. The anomaly C8, for example, could belong to the ISCB instead of the Serrinha Block. Indeed, in some inversions, including the one that uses the vertical field only (see Supplemental Material), this conductive feature has been positioned more to the west. Regarding the anomaly C9, it seems that it is spatially positioned near the transition, from north-south to east-west, in the structural orientation of the RIGB. The significance of this change

in structural orientation is still a matter of debate, but some authors have invoked anorogenic processes to explain its origin. Chauvet et al. (1997), for example, present a tectonic model in which the switch from contractional to strike-slip tectonic regimes in the RIGB was triggered by the ascent and emplacement of granodioritic plutons. However, the MT results show that there is significant similarity in terms of geometry and intensity of the anomalies in the southern part of RIGB with those from the central part. Therefore, we speculate that these anomalies may be associated with some nearly NE-SW-oriented collisional process within the Serrinha Block. This is consistent with the tectonic lineation of the Proterozoic rocks that outcrop just east of the Tucano Basin.

Some anomalies that appear as isolated bodies could in fact be continuous, but appear as distinct blobs due to the wide profile separation. A good example is the pair of anomalies (S1 and S2 in Fig. 6c) that occurs in the central-eastern part of the Serrinha Block. These conductive features are positioned approximately along a shear zone (Main Shear Zone; Chauvet et al. 1997) that has been considered to separate two distinct Archean basement subdomains (see Grisolia & Oliveira 2012). In fact, across the imaginary line connecting the pair of anomalies, the crust, as a whole, becomes more resistive to the west, reinforcing the association of these anomalies with a continuous geological discontinuity. This same observation regarding the continuity of isolated bodies can be applied to the conductors modeled in the ISCB. However, the conductive ISCB zone is almost certainly quite complex, with unresolved fine structure, and substantial macroscopic structural anisotropy. The imaged structures are likely a heavily smoothed of very complex structures. Additional MT sites would be required to resolve these questions.

Fig. 7 also displays a reduction in resistivity (anomaly D) at uppermost mantle depths. The top of the feature is located near the Moho at the central-eastern Serrinha Block. Its termination is abrupt to the west, whereas the anomaly becomes more diffuse to the east. All inversions have a lithosphere in the eastern part of the model that is about one order of magnitude more conductive than in the west,

with a possible resistivity discontinuity below the Serrinha Block. However, these deep structures need to be treated with caution given the results of the resolution tests discussed above. Long period data which could penetrate the conductive shallow structures imaged here would be required to resolve this deeper larger scale variation. Increasing aperture with longer profiles would also help resolve deeper structure.

7 CONCLUSIONS

Given the non-uniform distribution of sites, our MT dataset presents significant challenges for 3-D inversion. However, behavior of impedance phases, variable induction vector orientations and formal dimensionality analysis all provide strong evidence for predominance of 3-D geoelectric structure. Although many details (in particular along strike continuity of structures) are poorly resolved, the 3-D inversion nonetheless provides a reasonably coherent regional view of crustal conductivity structures and shed some light on the Paleoproterozoic collision of Archean blocks that gave rise to the current configuration of the São Francisco Craton basement. Our results also provide further evidence that 3-D inversions can fit out-of-quadrant phases without using anisotropy or fine scale structure that mimics anisotropy.

The strong crustal conductors that are mapped beneath the Serrinha Block most probably represent traces of tectonomagmatic processes that affected the São Francisco Craton during this Paleoproterozoic orogeny. The very high conductivities within the crust of the Serrinha Block most likely represent sulfides and/or carbon within a Paleoproterozoic suture zone. The geometry of these conductors suggests a westward vergent arc-continent collision. These observations support petrogenetic studies that advocate that the RIGB was formed in an island arc environment. Our results are the first direct geophysical evidence to support previous geological results that suggest the contact

between banded gneisses and the greenstone belt are probably trace an ancient continental margin that was active during the collision of the Rio Itapicuru Arc with the basement of the Serrinha Block.

ACKNOWLEDGMENTS

We thank the dedicated field and lab crew at INPE. This study was funded by the Brazilian National Research Council (CNPq) through the National Institute of Science and Technology for Tectonics Studies (INCT-ET, grant 713 573713/2008-1), UFBA/PETROBRAS Rift Project, the CNPq Millenium Institute grant 420 222/05-6 and CNPq grant 470.960/2004-3. MSB, ALP and IV also thank CNPq for research fellowships. MSB had a Post-Doctoral fellowship from CNPq (202368/2011-4) during his work. Partial computational support from Petrobras (grant 4600365494). Careful reviews from Kate Selway and one anonymous reviewer improved the original manuscript.

REFERENCES

- Aizawa, K., Koyama, T., Hase, H., Uyeshima, M., Kanda, W., Utsugi, M., Yoshimura, R., Yamaya, Y., Hashimoto, T., Yamazaki, K., Komatsu, S., Watanabe, A., Miyakawa, K. & Ogawa, Y., 2014. Three-dimensional resistivity structure and magma plumbing system of the Kirishima volcanoes as inferred from broadband magnetotelluric data, *J. Geophys. Res.*, **119**, 198-215.
- Almeida, F.F.M, Brito Neves, B.B. & Carneiro, C.D.R., 2000. The origin and evolution of the South American Platform, *Earth-Sci. Rev.*, **50**, 77-111.
- Barbosa, J.S.F. & Sabatè, P., 2004. Archean and Paleoproterozoic crust of the São Francisco Craton, Bahia, Brazil: geodynamic features, *Precambrian Res.*, **133**, 1-27, doi:10.1016/j.precamres.2004.03.001.
- Bizzi, L.A., Schobbenhaus, C., Vidotti, R.M. & Gonçalves, J.H., 2003. *Geologia, Tectônica e Recursos*

Minerais do Brasil, 692 pp. CPRM - Serviço Geológico do Brasil, Brasília.

Boerner, D.E., Kurtz, R.D. & Craven, J.A., 1996. Electrical conductivity and Paleo-Proterozoic foredeeps, *J. Geophys. Res.*, **101**, 13,775–13,791, doi:10.1029/96JB00171.

Brito Neves, B.B., Sial, A.N. & Albuquerque, J.P.T., 1977. Vergência centrífuga residual no Sistema de Dobramentos Sergipano, *Rev. Bras. Geoc.*, **7**, 102–114.

Chauvet, A., Da Silva, F.C.A., Faure, M. & Guerrot, C., 1997. Structural evolution of the Paleoproterozoic Rio Itapicuru granite-greenstone belt (Bahia, Brazil): the role of synkinematic plutons in the regional tectonics, *Precambrian Res.*, **84**, 139-162, doi:10.1016/s0301-9268(97)00024-7.

Costa, F.G., Oliveira, E.P. & McNaughton, N.J., 2011. The Fazenda Gavião granodiorite and associated potassic plutons as evidence for Palaeoproterozoic arc-continent collision in the Rio Itapicuru greenstone belt, Brazil, *J. S. Am. Earth Sci.*, **32**, 127-141, doi:10.1016/j.jsames.2011.04.012.

Cruz Filho, B., Conceição, H., Rios, D.C., Rosa, M.L.S. & Marinho, M.M., 2003. Geologia, petrografia e litogeoquímica do batólito trondhjemítico Nordestina, Núcleo Serrinha, nordeste da Bahia, *Rev. Bras. Geoc.*, **33**, 175-186.

Donatti-Filho, J.P., Tappe, S., Oliveira, E.P. & Heaman, L.M., 2013. Age and origin of the Neoproterozoic Brauna kimberlites: Melt generation within the metasomatized base of the São Francisco craton, Brazil, *Chem. Geol.*, **353**, 19-35, 10.1016/j.chemgeo.2012.06.004.

Egbert, G.D., 1997. Robust multiple-station magnetotelluric data processing, *Geophys. J. Int.*, **130**, 475-496, doi:10.1111/j.1365-246X.1997.tb05663.x.

Egbert, G.D. & Kelbert, A., 2012. Computational recipes for electromagnetic inverse problems,

Geophys. J. Int., **189**, 251-267, doi:10.1111/j.1365-246X.2011.05347.x.

Feng, M., van der Lee, S. & Assumpção, M., 2007. Upper mantle structure of South America from joint inversion of waveforms and fundamental mode group velocities of Rayleigh waves, *J. Geophys. Res.*, **112**, B04312, doi:10.1029/2006JB004449.

Figueiredo, M.C.H. 1989. Geochemical evolution of eastern Bahia, Brazil: a probable Early Proterozoic subduction-related magmatic arc, *J. S. Am. Earth Sci.*, **2**, 131- 145.

Gaal, G., Teixeira, J.B.G., D'el-Rey Silva, L.J.H., Silva, M.G., 1987. Early Proterozoic crustal evolution and metallogenesis, northwestern Bahia, Brazil, in *International Symposium on granites and metallogenesis*, Unpublished Conference at ISGAM, Salvador.

Grisolia, M.F.P. & Oliveira, E.P., 2012. Sediment provenance in the Palaeoproterozoic Rio Itapicuru greenstone belt, Brazil, indicates deposition on arc settings with a hidden 2.17-2.25 Ga substrate, *J. S. Am. Earth Sci.*, **38**, 89-109, doi:10.1016/j.jsames.2012.06.004.

Groom, R.W. & Bailey, R.C., 1989. Decomposition of magnetotelluric impedance tensors in the presence of local three-dimensional galvanic distortion, *J. Geophys. Res.*, **94**, 1913-1925, doi:10.1016/j.jsames.2012.06.004.

Gutscher, M.A., Maury, R., Eissen, J.P. & Bourdon, E., 2000. Can slab melting be caused by flat subduction? *Geology*, **28**, 535-538.

Heise, W. & Pous, J., 2003. Anomalous phases exceeding 90° in magnetotellurics: anisotropic model studies and a field example, *Geophys. J. Int.*, **155**, 308–318.

Ichihara H. & Mogi T., 2009. A realistic 3-D resistivity model explaining anomalous large magnetotelluric phases: the L-shaped conductor model, *Geophys. J. Int.*, **179**, 14-17.

Jones, A.G., 1992. Electrical conductivity of the continental lower crust, in *Continental Lower Crust*,

pp. 81–143, ed. Fountain, D.M., Arculus, R.J. & Kay, R.W., Elsevier.

Jones, A.G., 1993. Electromagnetic images of modern and ancient subduction zones, *Tectonophysics*, **219**, 29-45, doi:10.1016/0040-1951(93)90285-R.

Jones, A.G., 2012. Distortion of magnetotelluric data: its identification and removal, in *The Magnetotelluric Method: Theory and Practice*, pp. 219-302, ed. Chave, A. & Jones, A.G., Cambridge University Press.

Karner, G.D., Egan, S.S. & Weissel, J.K., 1992. Modeling the tectonic development of the Tucano and Sergipe-Alagoas rift basins, Brazil, *Tectonophysics*, **215**, 133-160, doi:10.1016/0040-1951(92)90078-k.

Kelbert, A., Meqbel, N., Egbert, G.D. & Tandon, K., 2014. ModEM: A modular system for inversion of electromagnetic geophysical data, *Comput. Geosci.*, **66**, 40-53, doi:10.1016/j.cageo.2014.01.010.

Korja, T. & Hjelt, S.E., 1993. Electromagnetic studies in the Fennoscandian Shield--electrical conductivity of Precambrian crust, *Phys. Earth Planet. In.*, **81**, 107-138.

Kuhn, C., Kuster, J. & Brasse, H., 2014. Three-dimensional inversion of magnetotelluric data from the Central Andean continental margin, *Earth Planets Space*, **66**, doi: 10.1186/1880-5981-66-112.

Magnavita, L.P., Davison, I. & Kusznir, N.J., 1994. Rifting, erosion, and uplift history of the Reconcavo-Tucano-Jatoba Rift, Northeast Brazil, *Tectonics*, **13**, 367-388, doi:10.1029/93tc02941.

Matos, F.M.V & Conceição, H., 1993. Granitogênese associada à parte oeste do Cráton Serrinha e o Greenstone Belt do Rio Itapicuru: Geologia e Tipologia, in *II Simpósio do Cráton do São Francisco*, Anais, pp. 60-62, SBG/SGM/CNPq.

McNeice, G.W. & Jones, A.G., 2001. Multisite, multifrequency tensor decomposition of magnetotelluric data, *Geophysics*, **66**, 158-173.

- Milani, E.J. & Davison, I., 1988. Basement control and transfer tectonics in the Recancavo-Tucano-Jatoba rift, Northeast Brazil, *Tectonophysics*, **154**, 41-70, doi:10.1016/0040-1951(88)90227-2.
- Nover, G., 2005. Electrical properties of crustal and mantle rocks - A review of laboratory measurements and their explanation, *Surv. Geophys.*, **26**, 593-651, doi:10.1007/s10712-005-1759-6.
- Oliveira, E. P., Escayola, M., Souza, Z. S., Bueno, J. F., Araujo, M. G. S. & McNaughton, N., 2007. The Santa Luz chromite-peridotite and associated mafic dykes, Bahia-Brazil: remnants of a transitional type ophiolite related to the Palaeoproterozoic (>2.1 Ga) Rio Itapicuru greenstone belt? *Rev. Bras. Geoci.*, Supplement 4, **37**, 28-39.
- Oliveira, E.P., McNaughton, N.J. & Armstrong, R., 2010. Mesoarchaeon to Palaeoproterozoic growth of the northern segment of the Itabuna–Salvador–Curaçá orogen, São Francisco craton, Brazil, in *The Evolving Continents: Understanding Processes of Continental Growth*, pp. 263-286, ed. Kusky, T.M., Zhai, M.G. & Xiao, W., Geological Society of London.
- Padilha, A.L., Vitorello, Í., Pádua, M.B. & Fuck, R.A., 2016. Deep magnetotelluric signatures of the early Neoproterozoic Cariris Velhos tectonic event within the Transversal sub-province of the Borborema Province, NE Brazil, *Precambrian Res.*, **275**, 70-83, doi:10.1016/j.precamres.2015.12.012.
- Pek, J. & Verner, T., 1997. Finite-difference modelling of magneto-telluric fields in two-dimensional anisotropic media, *Geophys. J. Int.*, **128**, 505–521.
- Rios, D.C., Davis, D.W., Conceição, H., Davis, W.J., Rosa, M.L.S. & Dickin, A.P., 2009. Geologic evolution of the Serrinha nucleus granite-greenstone terrane (NE Bahia, Brazil) constrained by U-Pb single zircon geochronology, *Precambrian Res.*, **170**, 175-201, doi:10.1016/j.precamres.2008.10.001.

- Ruggiero, A. & Oliveira, E. P., 2010. Caracterização de vulcânicas adakíticas e cálcio-alcalinas no greenstone belt do rio Itapicuru, Bahia: petrogênese e implicações geodinâmicas, *Rev. Bras. Geoci.*, **40**, 1-18.
- Selway, K., 2014. On the causes of electrical conductivity anomalies in tectonically stable lithosphere, *Surv. Geophys.*, **35**, 219-257, doi:10.1007/s10712-013-9235-1.
- Silva, M. G., 1992. O greenstone belt do Rio Itapicuru: uma bacia do tipo back-arc fossil, *Rev. Bras. Geoci.*, **22**, 157-166.
- Smithies, R.H., Champion, D.C. & Cassidy, K.F., 2003. Formation of earth's early Archaean continental crust, *Precambrian Res.*, **127**, 89-101, doi:10.1016/s0301-9268(03)00182-7.
- Teixeira, W., Sabatè, P., Barbosa, J., Noce, C.M. & Carneiro, M.A., 2000. Archean and Paleoproterozoic evolution of the São Francisco Craton, Brazil, in *Tectonic Evolution of South America*, ed. Cordani, U.G., Milani, E.J., Thomaz Filho, A. & Campos, D.A., pp. 101–137, Sociedade Brasileira de Geologia.
- Unsworth, M., 2010. Magnetotelluric studies of active continent-continent collisions, *Surv. Geophys.*, **31**, 137-161, doi:10.1007/s10712-009-9086-y.
- Ussami, N., Karner, G.D. & Bott, M.H.P., 1986. Crustal detachment during South Atlantic rifting and formation of Tucano - Gabon basin system, *Nature*, **322**, 629-632, doi:10.1038/322629a0.
- Vitarello, Í., Padilha, A.L., Santos, A.C.L., Pádua, M.B., Fontes, S.L., Bologna, M.S. & Fuck, R.A., 2013. Electromagnetic induction studies in the Borborema Province and adjacent terrains, northeastern Brazil: 2013-INCTET progress report, in *13th International Congress of the Brazilian Geophysical Society & EXPOGEF*, Expanded Abstracts, pp. 914-917, SBGf.
- Wannamaker, P.E., 2005. Anisotropy versus heterogeneity in continental solid earth electromagnetic

studies: Fundamental response characteristics and implications for physicochemical state, *Surveys in Geophysics*, **26**, 733-765.

Weckmann, U., Ritter, O. & Haak, V., 2003. A magnetotelluric study of the Damara belt in Namibia – 2. MT phases over 90° reveal the internal structure of the Waterberg Fault/Omaruru Lineament, *Phys. Earth Planet. Int.*, **138**, 91–112.

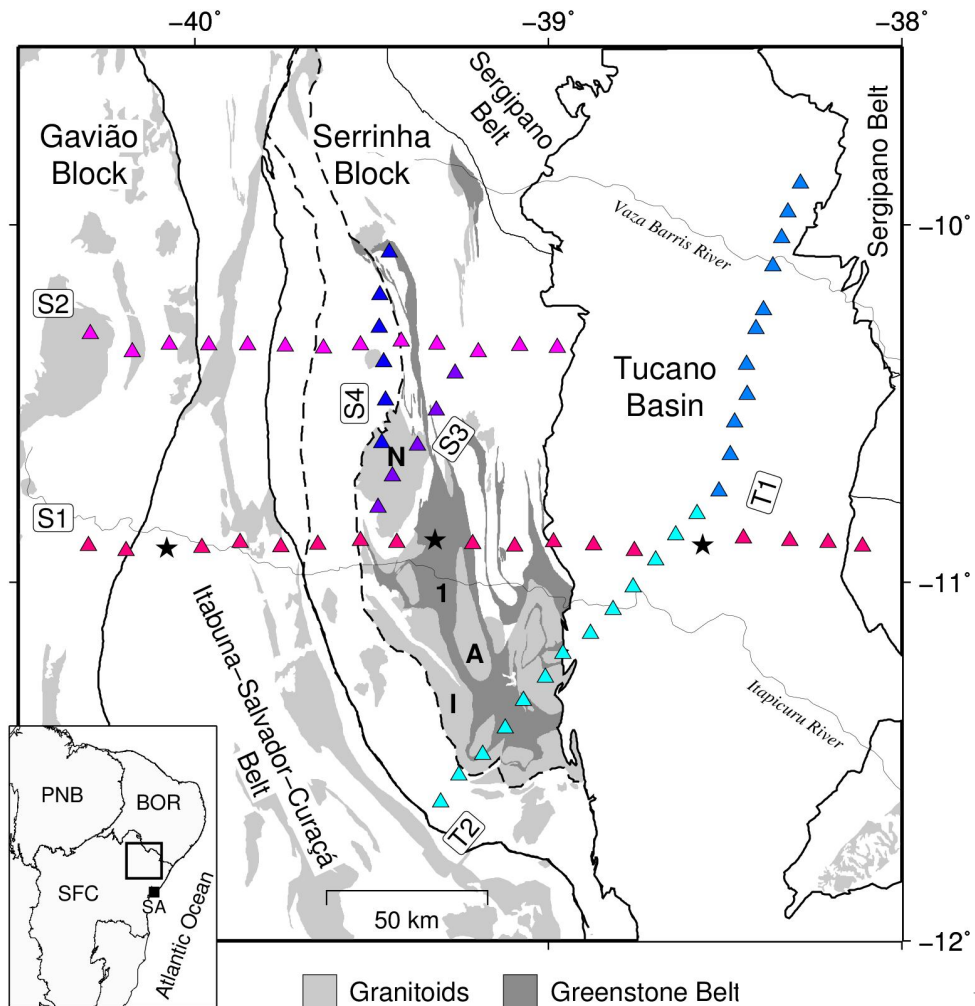


Figure 1. The

68 MT sites (triangles and stars) distributed along six linear profiles (S1, S2, S3, S4, T1 and T2) deployed in northeastern São Francisco Craton over the simplified geological map (modified from Bizzi et al. 2003). Stars indicate, from left to right, the sites ser004a, ser010a and ser017a, whose responses are displayed in Fig. 2. Greenstone belts: 1. Rio Itapicuru (RIGB). Granitoids: I, Itareru tonalite; N, Nordestina Batholith; A, Ambrósio Dome. Acronyms in inset figure are: BOR, Borborema Province; PNB, Parnaíba Basin; SA, Salvador City; SFC, São Francisco Craton.

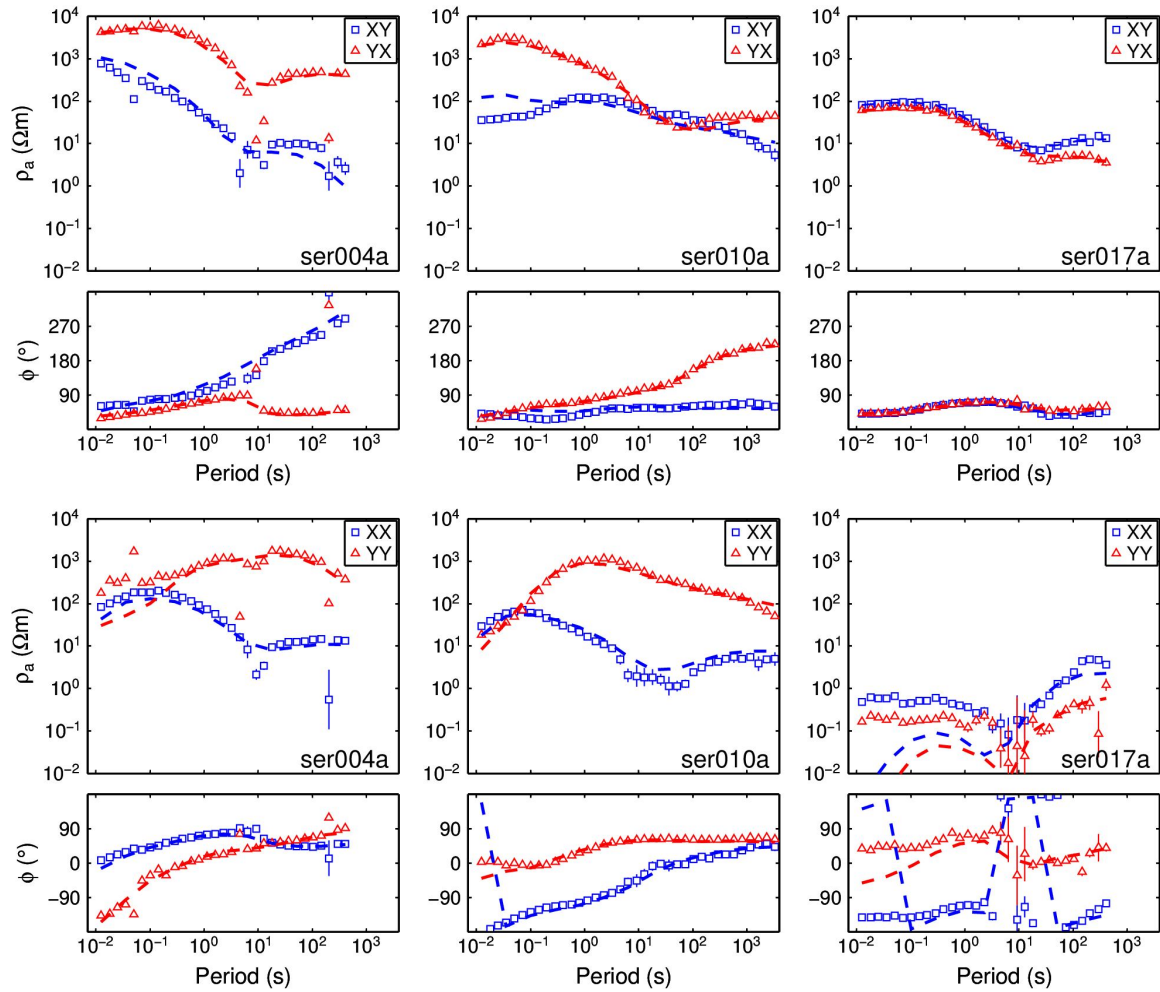
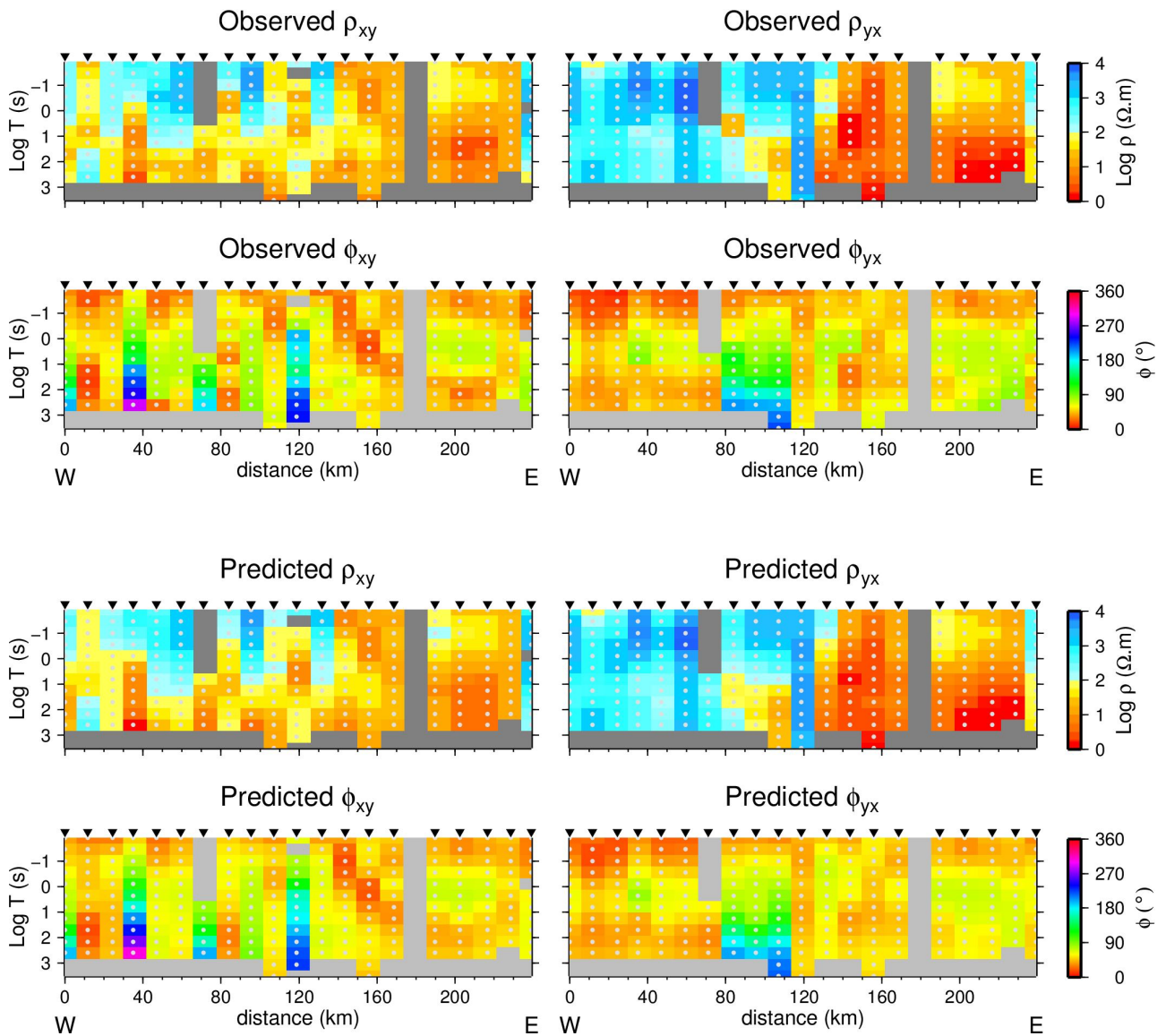


Figure 2. Apparent resistivity and phase of three representative sites (location shown as stars in Fig.1) with the x -axis rotated to the geographic north. Site ser004a is on the Itabuna-Salvador-Curaçá Belt (ISCB), in the western part of the study area. Site ser010a is representative of the Serrinha Block, in the central part of the region, whereas site ser017a is a typical response from the sedimentary Tucano Basin. The upper panel displays the off-diagonal components. We can observe the xy - and yx -component phases leaving the quadrant at sites ser004a and ser010a, respectively. At site ser017a, responses are almost 1-D for most part of the data. The lower panel shows the diagonal components. It can be seen that the diagonal components are very well resolved for the sites ser001a and ser010a. In the basin, as expected, diagonal responses are very weak. Dashed lines are the



predicted responses from the 3-D inversion using ModEM code.

Figure 3. Pseudo-sections of apparent resistivity and phase data along the profile S1. The left and right columns give the xy and yx modes, respectively. The yx -component phases have been shifted by 180° . The top four pseudo-sections are the measured responses with the x -axis rotated to the geographic north, whereas the bottom four are the calculated responses for the preferred inversion model.

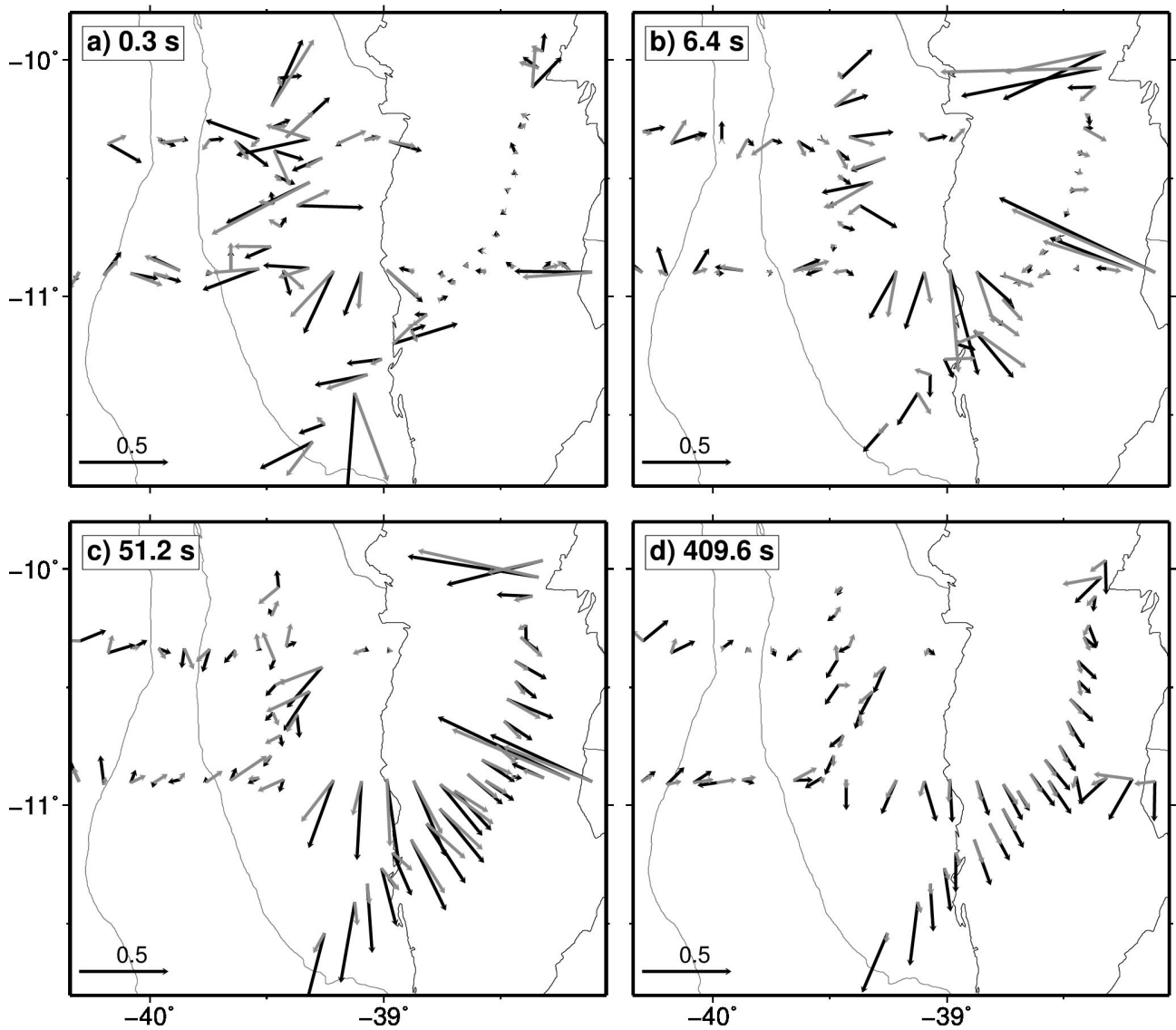


Figure 4. Real induction vectors using Parkinson convention (vectors point toward induced internal currents) for periods of 0.3, 64, 51.2 and 409.6 s. Black arrows are the observed induction vectors derived from single-station vertical field transfer functions, whereas gray arrows are the induction vectors predicted by the preferred 3-D inversion model, which results from jointly inverting \mathbf{Z} and VTFs. Fits to induction vectors, however, are similar for the joint and VTF-only inversions.

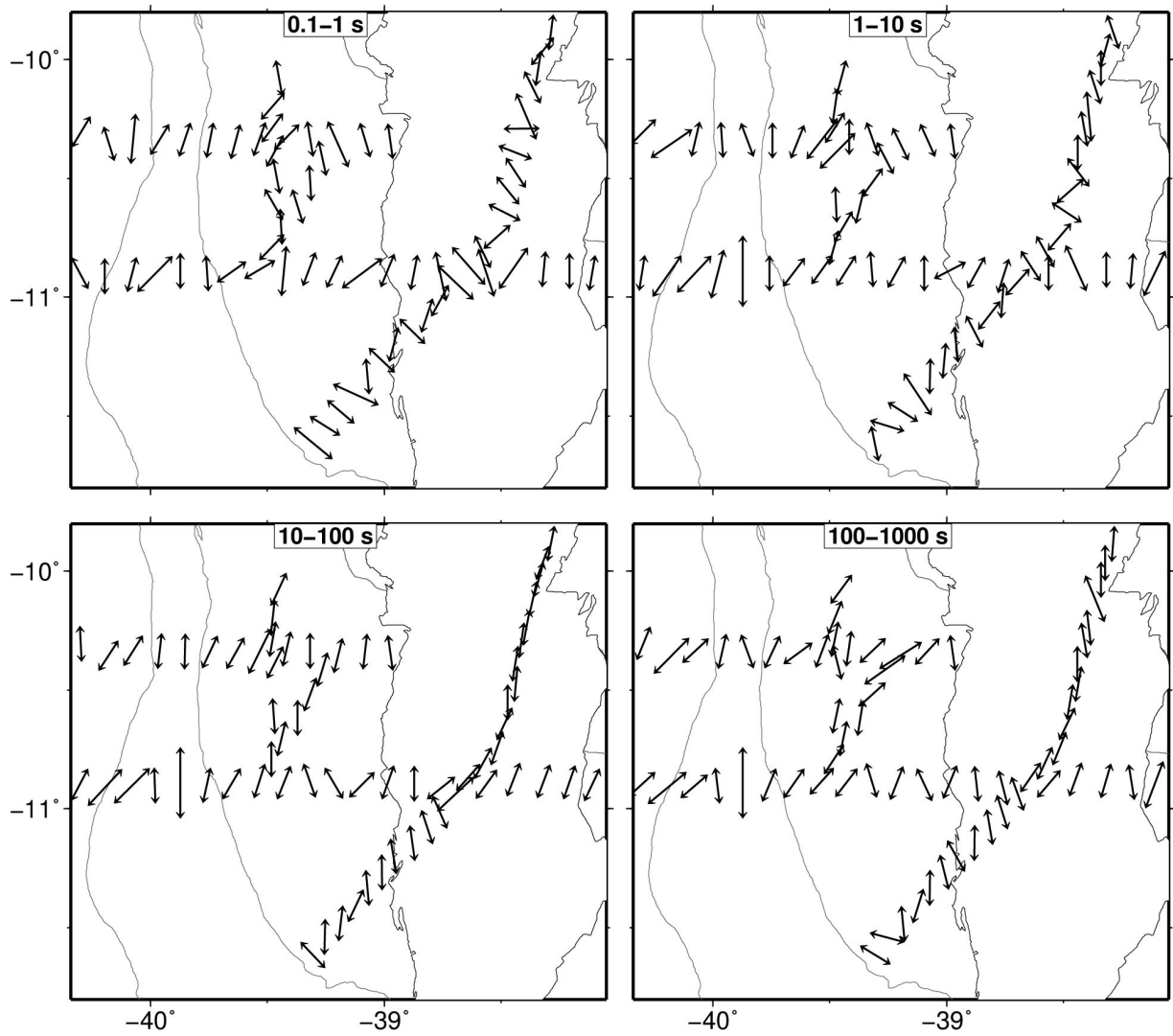


Figure 5. Unconstrained geoelectric strike directions given by fitting the distortion model of Groom & Bailey (1989) using the code of McNeice & Jones (2001) for four period bands.

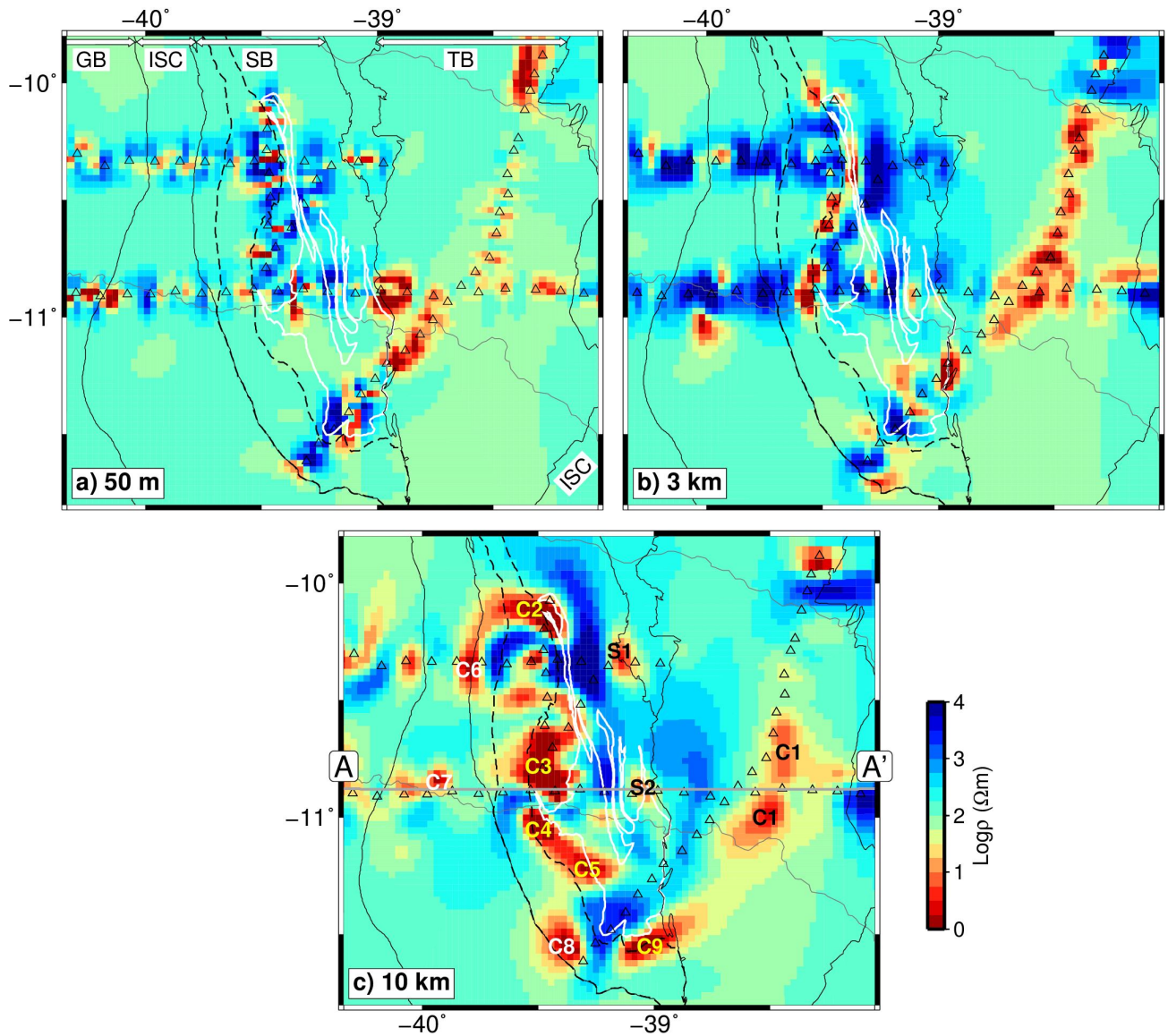


Figure 6. Preferred inverse model at representative depths: 50 m (a), 3 km (b) and 10 km (c). Features C1-C9 are conductive anomalies discussed in the text. Gray straight line in Fig. 6c indicates location of the profile plotted in Fig. 7. GB: Gavião Block; ISC: Itabuna-Salvador-Curaçá Belt; SB: Serrinha Block; TB: Tucano Basin.

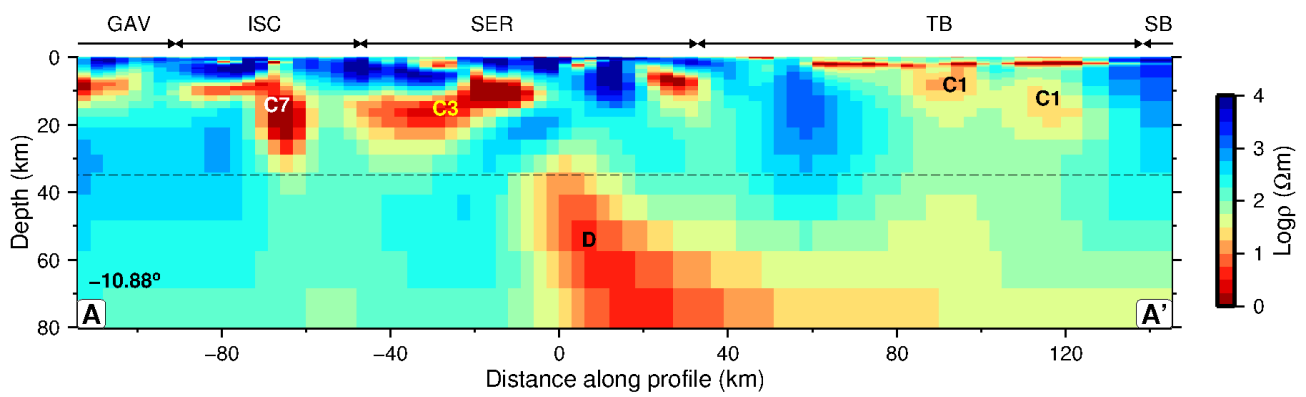


Figure 7. Representative east-west cross section along the latitude -10.88° (line A-A' in Fig. 6c) showing some of the main features identified in the preferred model. Dashed black line is the average Moho calculated by using regional depth values from Feng et al. (2007). GAV, Gavião Block; ISC, Itabuna-Salvador-Curaçá Belt; SER, Serrinha Block; TB, Tucano Basin; SB, Sergipano Belt.

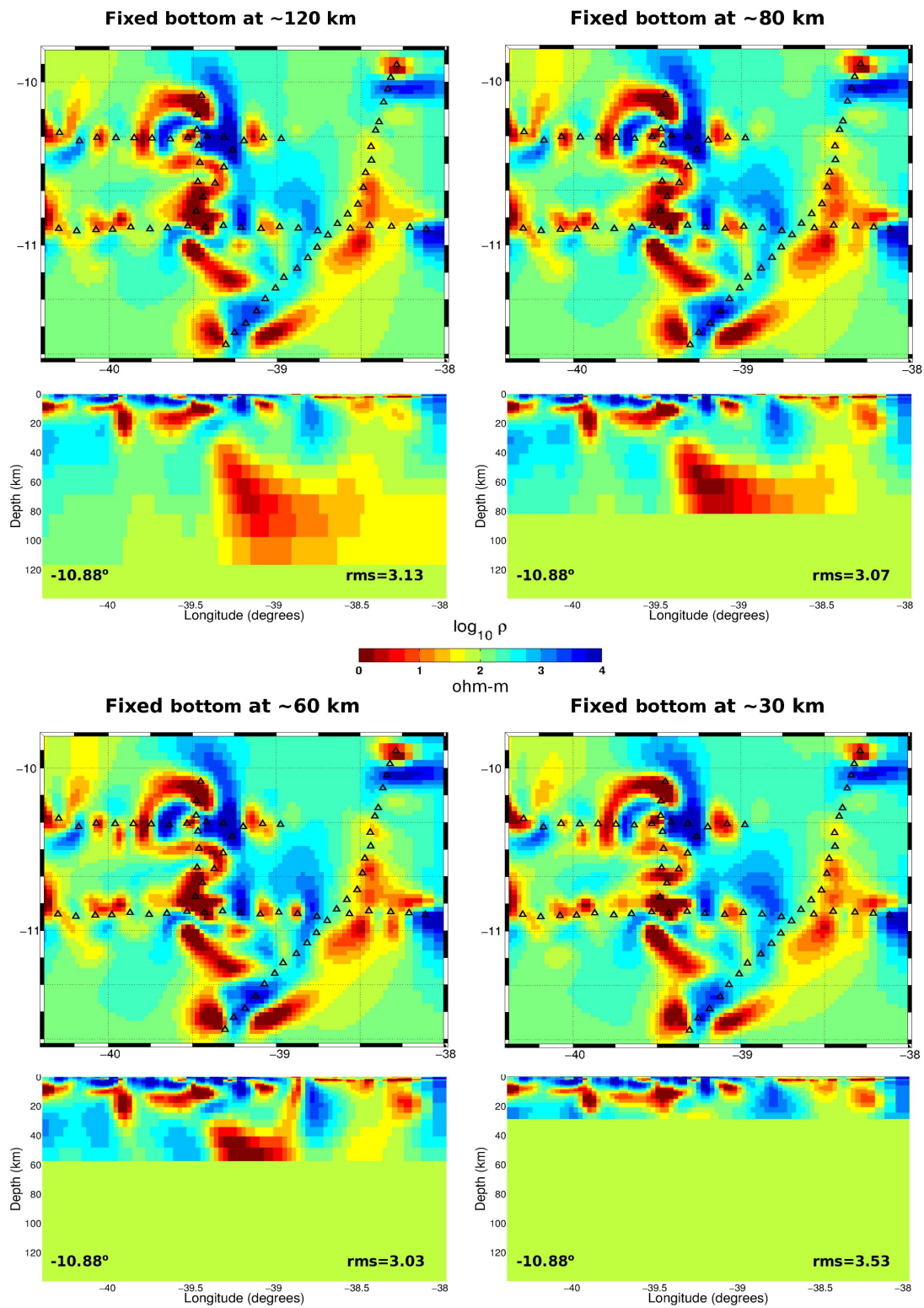


Figure 8. Horizontal slices at 10 km depth and east-west cross sections at latitude -10.88° obtained with model

resistivity fixed for different depths. See text for discussion.

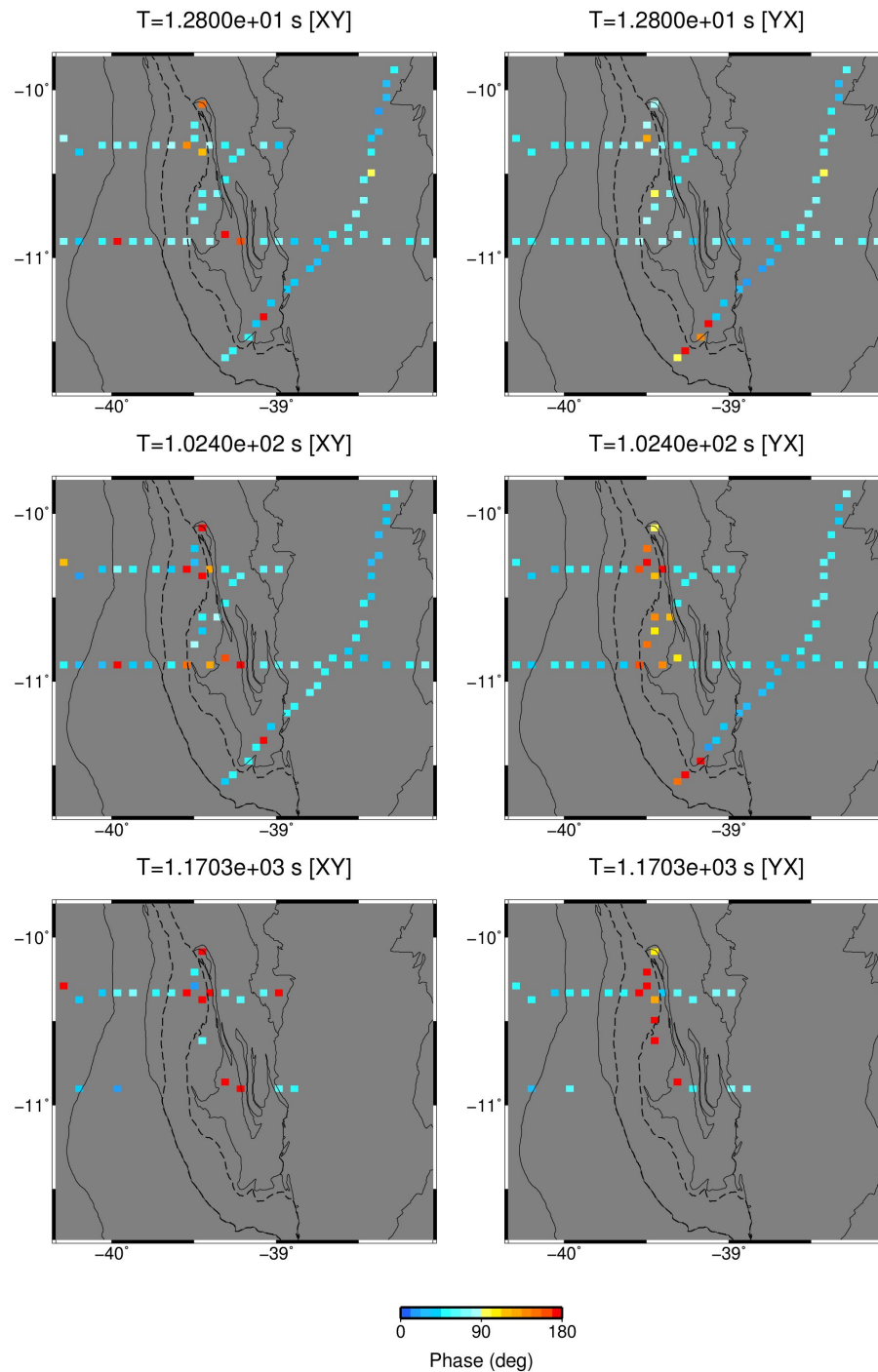


Figure 9. Maps of the measured phases rotated to N23°W at selected periods. The left and right columns give the xy and yx modes, respectively. The yx -component phases have been shifted by 180°. Out-of-quadrant phases appear mainly over the complex buried conductive features of the Serrinha Block, indicating a relationship of the

anomalous phases with the conductive structures.

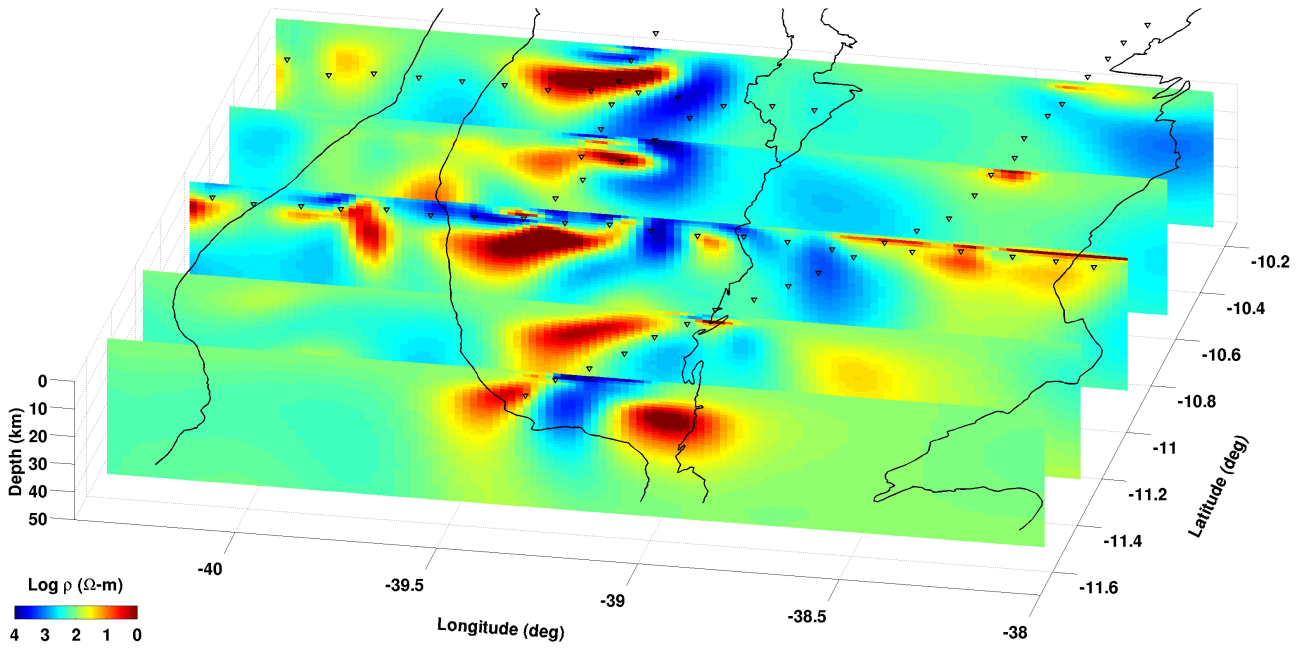


Figure 10. Perspective view of the 3-D inversion model. Solid black lines indicate, from left to right, the surficial limits of the Gavião Block, Itabuna-Salvador-Curaçá Belt (ISCB), Serrinha Block, Sergipano Belt and Tucano Basin, marked as in Fig. 1. Triangles denote the MT site positions.